Polymer 52 (2011) 5075–5084

Contents lists available at SciVerse ScienceDirect

Polymer

journal homepage: www.elsevier.com/locate/polymer

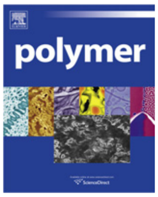

Synthesis and characterization of side-chain liquid crystalline polymers and oriented elastomers containing terminal perfluorocarbon chains

Fan-Bao Meng*, Xiao-Dong Zhang, Xiao-Zhi He, He Lu, Yue Ma, Hui-Li Han, Bao-Yan Zhang

Research Center for Molecular Science and Engineering, Northeastern University, Shenyang 110004, PR China

A R T I C L E I N F O

Article history:
Received 22 February 2011
Received in revised form
23 July 2011
Accepted 4 September 2011
Available online 10 September 2011

Keywords:
Liquid crystalline polymers
Elastomers
Fluoropolymers

A B S T R A C T

Several novel chiral side-chain liquid crystalline (LC) polysiloxane resins containing epoxy groups and mesogenic components have been graft copolymerized by a one-step hydrosilylation reaction with poly(methylhydrogeno)siloxane, an epoxy monomer 2-(allyloxymethyl)oxirane, and chiral fluorinated liquid-crystalline monomers 4′-(4-(allyloxy)benzoyloxy)biphenyl-4-yl 6-(perfluorooctanoyloxy)hexahydrofuro[3,2-*b*]furan-3-yl adipate and 4′-(4-(undec-10-enoyloxy)benzoyloxy)biphenyl-4-yl 6-(perfluorooctanoyloxy)hexahydrofuro[3,2-*b*]furan-3-yl adipate. The synthesized epoxy resins are cured using 4,4′-diaminodiphenyl-methane in mesophase state under a magnetic field to obtain crosslinked oriented elastomers. The chemical structures, LC properties and surface morphology of the monomers, the resins and the liquid crystalline elastomers (LCEs) are characterized by use of various experimental techniques such as FTIR, ^{1}H NMR, EA, TGA, DSC, POM, and X-ray measurements. The mesomorphic properties of the synthesized resins and corresponding oriented elastomers are influenced by the terminal perfluorocarbon chains components effectively. The resins show chiral nematic and chiral smectic C phases (S_c^*), and S_c^* are frozen in their corresponding oriented elastomers. The LC phases are verified by X-ray measurements, and the orientational order parameters of the oriented LCEs are calculated as well.

1. Introduction

Liquid crystal elastomers (LCEs) combine the orientational ordering properties of liquid crystalline systems with the rubbery elasticity of polymer networks, and have been developed as promising functional materials in recent years due to their remarkable properties such as interesting mechanical, electrical, and optical properties [1–5]. For the rubbery elasticity of LCEs, coupling between the polymer chain and side-groups and restricting the relative motion of polymer chains must be considered, and the LC behaviors of LCEs can be manifested by the mesogens and orientation. The orientation of the mesogens can be controlled through mechanical stress [6,7], as well as by electric and magnetic field [8–12]. Various mesogens have been introduced into the polymer networks for different application considerations through chemical design [13–15] and many papers recently appear dealing with mechanical, dynamic-mechanical and rheological properties of LCEs both on polydomain samples (in which the mesogenic groups are macroscopically disordered) and on monodomain samples (in which the mesogenic groups are macroscopically ordered) [16–20]. Chiral smectic C (S_c^*) liquid crystal is one of the most fantastic LC phases since it can form helical structure. S_c^* elastomers have attracted interest in both industrial and scientific fields due to their additional properties such as ferroelectricity, piezoelectricity and pyroelectricity [21–23]. In particular, the oriented S_c^* elastomers including monodomain LCEs are ideal materials for the investigation of piezoelectric and inverse piezoelectric effects in chiral smectic C systems because of macroscopic ordering of mesogenic groups and non-macroscopic flow in the polymer network matrix, because the macroscopic flow destroys piezoelectricity in conventional low-molar mass ferroelectric liquid crystals [24].

Recently, the use of organo-fluorine compounds has generated much research effort. Initial studies on fluorinated liquid crystals focused on partly fluorinated alkanes (i.e. diblock hydrocarbon-fluorocarbon molecules) [25]. Fluorocarbons and hydrocarbons are poorly miscible because the conformation and electrostatic interactions of the fluorocarbons are different from those of hydrocarbons. The formation of liquid-crystalline mesophases is due to the strong phase separation of fluorocarbon from hydrocarbon chain segments and the rigid-rod-like nature of the fluorocarbon chains which tend to adopt a helical conformation in the mesophase state [26,27]. Some synthetic efforts have subsequently resulted in the development of fluorinated liquid crystalline

---

* Corresponding author. Tel./fax: +86 24 83687671.
E-mail address: mengfb@mail.neu.edu.cn (F.-B. Meng).

0032-3861/$ – see front matter © 2011 Elsevier Ltd. All rights reserved.
doi:10.1016/j.polymer.2011.09.002

polymers in which the length of the fluorinated tail is varied. More conventional mesogenic units have also been used in combination with partly fluorinated tails in polymeric liquid crystals [28,29]. One can see chiral groups can form helical conformation, and some fluorocarbon-hydrocarbon systems tend to adopt a helical conformation in the mesophase state. Despite the studies reported so far, the details of elastomers containing both fluorocarbons and chiral groups are still unknown. In order to obtain a well-ordered and immobilized oriented LCEs at room temperature, and to study LCE systems bearing both fluorocarbons and chiral groups, we have recently succeeded in obtaining oriented S_c^* elastomers by curing resins with isosorbide and terminal perfluorocarbon chains under a magnetic field.

2. Experimental

2.1. Materials and methods

Poly(methylhydrogeno)siloxane (**PMHS**, $M_n \approx 2300$), 2-(allyloxymethyl)oxirane (**AMO**), 4,4′-diaminodiphenyl-methane (**DDM**) and 2,2,3,3,4,4,5,5,6,6,7,7,8,8,8-pentadecafluorooctanoic acid are obtained from ALDRICH without any further purification. 4′-hydroxybiphenyl-4-yl 4-(allyloxy)benzoate and 4′-hydroxybiphenyl-4-yl 4-(undec-10-enoyloxy)benzoate are synthesized according to previous reported procedure [30]. Biphenyl-4,4′-diol, undec-10-enoic acid, 3-bromopropene, isosorbide, adipic acid, hexachloroplatinic acid hydrate and reagent-grade solvents are obtained from Jilin Chemical Industry Company and used without any further purification. Tetrahydrofuran (THF) is dried over sodium metal and distilled. Pyridine is purified by distillation over KOH and NaH before using. Other reagent-grade solvents are used as received.

DSC and TGA measurements are carried out with a NETZSCH TGA 209C thermogravimetric analyzer, and a NETZSCH instruments DSC 204 (Netzsch, Wittelbacherstrasse, Germany) at a scanning rate of 10 °C min^{-1} under a flow of dry nitrogen. X-ray measurements is performed using Cu Kα ($\lambda = 1.542$ Å) radiation monochromatized with a Rigaku DMAX-3A X-ray diffractometer (Rigaku, Japan). The X-ray measurements include wide-angle X-ray diffraction (WAXD) experiments and small-angle X-ray scattering (SAXS) measurements. ^1H NMR, FTIR and element analyses (EA) are measured by Varian WH-90PFT NMR Spectrometer (Varian Associates, Palo Alto, CA), PerkinElmer instruments Spectrum One Spectrometer (PerkinElmer, Foster City, CA) and Elementar Vario EL III (Elementar, Germany), respectively. Measurement of optical rotation (α) is carried out with a PerkinElmer instrument Model 341 Polarimeter at room temperatures using sodium light source ($\lambda = 589$ nm). The polarized optical microscopy (POM) study is performed using a Leica DMRX (Leica, Wetzlar, Germany) equipped with a Linkam THMSE-600 (Linkam, Surrey, England) heating stage. The magnetic fields for curing samples are carried out with a SA-4602 type electromagnet provided by Shenyang Changcheng Electromagnet Manufacture Co (Yuhong, Shenyang, China).

2.2. Synthesis of the liquid crystalline monomers

Fig. 1 shows the synthesis routes of chiral liquid crystalline monomers 4′-(4-(allyloxy)benzoyloxy)biphenyl-4-yl 6-(perfluorooctanoyloxy)hexahydrofuro[*3,2-b*]furan-3-yl adipate (**ABPHA**).

Adipoyl dichloride (18.3 g, 0.1 mol), 200 mL chloroform are added into a round flask. It is added dropwise with solution of compound 4′-hydroxybiphenyl-4-yl 4-(allyloxy)benzoate (***1***) (6.93 g, 0.02 mol, dissolved in 150 mL dry chloroform) and 10 mL pyridine. The reaction mixture is stirred at 65 °C for 24 h. The solvent and excess adipoyl dichloride is distilled using a rotatory evaporator under reduced pressure. After cooling to room temperature, the mixture is poured into 100 mL cold water and acidified with 6 N sulfuric acid. The precipitates are isolated by filtration and recrystallized in ethanol and dried in a vacuum oven to obtain white crystals of 6-(4′-(4-(allyloxy)benzoyloxy)biphenyl-4-yloxy)-6-oxohexanoic acid (***2***). Yield: 87%. m.p.: 162 °C. IR (KBr, cm^{-1}): 3054, 2922, 2850 (CH_3, $-CH_2-$ and $-CH-$), 2648–2529 ($-OH$ in $-COOH$), 1751–1685 ($C{=}O$), 1639 ($C{=}C$ on terminal olefinic group), 1608, 1495 (Ar), 1293 ($C-O-C$). Anal. Calcd for $C_{28}H_{26}O_7$: C, 70.87%; H, 5.52%. Found: C, 70.78%; H, 5.59%. ^1H NMR ($CDCl_3$, δ, ppm): 1.21–1.58 [m, 4H, $-OOCCH_2(C\underline{H}_2)_2CH_2COOH$]; 2.16–2.39 [m, 4H, $-OOCC\underline{H}_2(CH_2)_2C\underline{H}_2COOH$]; 4.39–4.63 [d, 2H, $CH_2{=}CHC\underline{H}_2O-$]; 4.73–5.08 (m, 2H, $C\underline{H}_2{=}CH-$); 5.91–6.18 (m, 1H, $CH_2{=}C\underline{H}-$); 7.13–8.11 (m, 12H, $Ar-\underline{H}$); 12.03–12.21 (S, 1H, $-COO\underline{H}$).

The intermediate ***2*** (23.7 g, 0.05 mol), 50 mL thionyl chloride and 1.0 mL of pyridine are added into a round flask equipped with a catheter to absorb hydrogen chloride. The mixture is stirred at room temperature for 3 h, then heated to 60 °C and kept for 10 h in a water bath to ensure that the reaction finished. The excess thionyl chloride is distilled under reduced pressure. Then 100 mL cold THF is added to the residue at 25 °C to obtain THF solution of 4′-(6-chloro-6-oxohexanoyloxy)biphenyl-4-yl 4-(allyloxy)benzoate (***3***).

Isosorbide (43.8 g, 0.3 mol) and 18 mL pyridine are dissolved in 300 mL dry THF. To the solution, it is added dropwise with THF solution of ***3***. The reaction mixture is stirred at 65 °C for 36 h. The solvent is distilled out partly under reduced pressure. After cooling to room temperature, the residue is poured into 500 mL cold water. The precipitates are isolated by filtration, washed by hot water and dried in a vaccum oven. Recrystallization in alcohol results in white crystals of 4′-(4-(allyloxy)benzoyloxy)biphenyl-4-yl 6-hydroxyhexahydrofuro[*3,2-b*]furan-3-yl adipate (***4***). Yield: 63%. m.p.: 93 °C. IR (KBr, cm^{-1}): 3405 ($-OH$), 3076, 2935, 2871 (CH_3, $-CH_2-$, $-CH-$ and $Ar-H$), 1756–1722 ($C{=}O$), 1605, 1494 (Ar), 1292, 1256, 1167 ($C-O$). Anal. Calcd for $C_{34}H_{34}O_{10}$: C, 67.76%; H, 5.69%. Found: C, 67.83%; H, 5.62%. ^1H NMR ($CDCl_3$, δ, ppm): 1.27–1.59 [m, 4H, $-OOCCH_2(C\underline{H}_2)_2CH_2COO-$]; 2.21–2.38 [m, 4H, $-OOCC\underline{H}_2(CH_2)_2C\underline{H}_2COO-$]; 3.69–4.68 [m, 10H, $CH_2{=}CHC\underline{H}_2O-$, and $-C\underline{H}_2-O-$ or

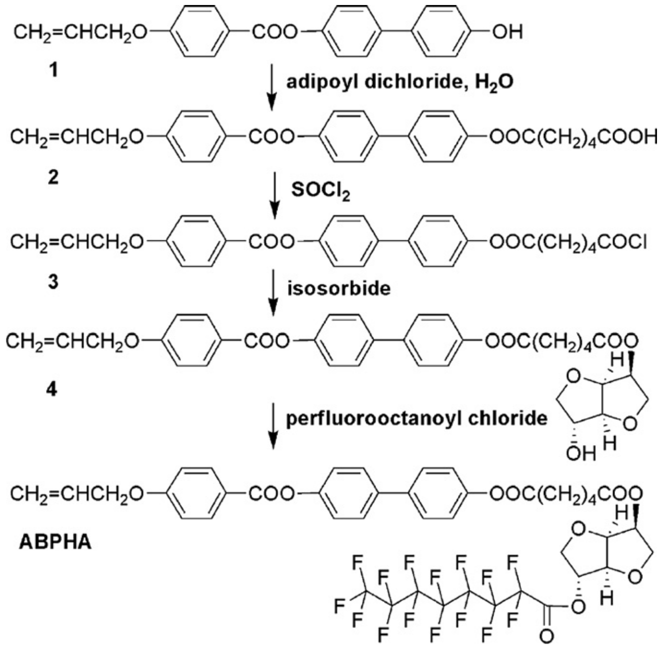

Fig. 1. Synthetic routes to monomers 4′-(4-(allyloxy)benzoyloxy)biphenyl-4-yl 6-(perfluorooctanoyloxy)hexahydrofuro[*3,2-b*]furan-3-yl adipate (ABPHA).

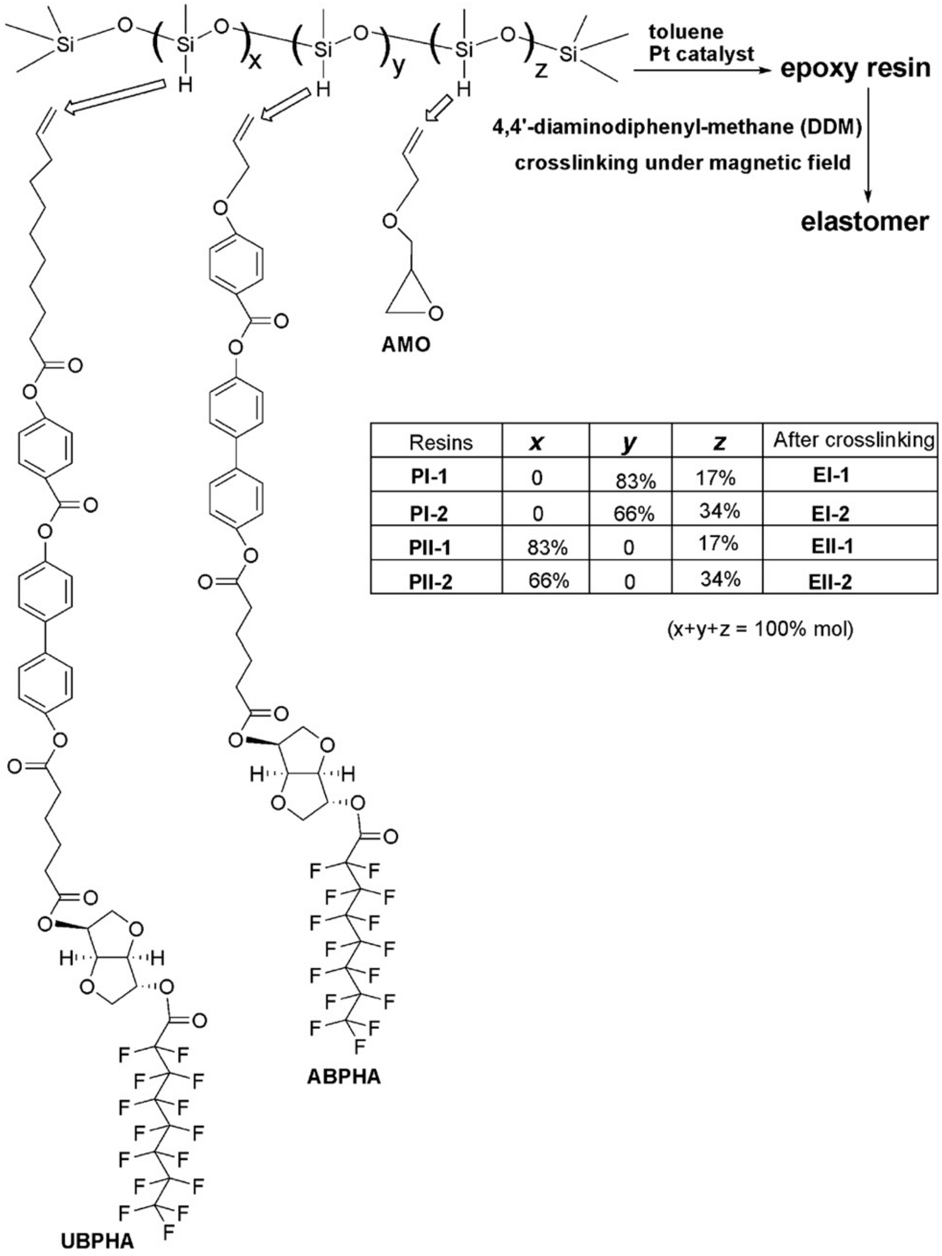

Resins	*x*	*y*	*z*	After crosslinking
PI-1	0	83%	17%	EI-1
PI-2	0	66%	34%	EI-2
PII-1	83%	0	17%	EII-1
PII-2	66%	0	34%	EII-2

Fig. 2. Synthetic route to resins and elastomers.

$-C\underline{H}-O-$ in isosorbide group]; 4.93−5.16 (m, 2H, $C\underline{H}_2{=}CH-$); 5.90−6.17 (m, 1H, $CH_2{=}C\underline{H}-$); 7.11−8.14 (m, 12H, Ar−$\underline{H}$); 9.45−9.69 (S, 1H, $-O\underline{H}$).

Compound ***4*** (30.1 g, 0.05 mol) and 10.0 mL dry pyridine are dissolved in 250 mL dry THF to form a solution. Perfluorooctanoyl chloride (21.6 g, 0.05 mol) is added dropwise to the solution and reacted at 63 °C for 48 h; then some solvent is distilled out. The mixture is cooled, poured in 600 mL cold water. The precipitated crude product is filtered, washed with hot water, recrystallized with alcohol and dried overnight under vacuum to obtain a white powder of liquid-crystalline monomer **ABPHA**. Yield: 53%. $[\alpha]_D^{20} = +41.1°$, $c = 1$, chloroform; m.p.: 64.4 °C. IR (KBr, cm^{-1}): 3074, 2926, 2851 (CH_3-, $-CH_2$-, −CH− and Ar−H), 1755−1724 (C=O), 1608, 1510 (Ar), 1293, 1259, 1213, 1170 (C−O), 1149 (C−F). Anal. Calcd for $C_{42}H_{33}F_{15}O_{11}$: C, 50.51%; H, 3.33%. Found: C, 50.63%; H, 3.29%. ^{1}H NMR ($CDCl_3$, δ, ppm): 1.32−1.70 [m, 4H, $-OOCCH_2(C\underline{H}_2)_2CH_2COO-$]; 2.51−2.61 [m, 4H, $-OOCC\underline{H}_2(CH_2)_2C\underline{H}_2COO-$]; 3.68−4.47 [m, 8H, $-C\underline{H}_2-O-$ and $-C\underline{H}-O-$ in isosorbide group]; 4.59−4.65 [d, 2H, $CH_2{=}CHC\underline{H}_2O-$]; 5.26−5.51 (m, 2H, $C\underline{H}_2{=}CH-$); 6.05−6.18 (m, 1H, $CH_2{=}C\underline{H}-$); 7.05−8.17 (m, 12H, Ar−$\underline{H}$).

The synthesis scheme of 4′-(4-(undec-10-enoyloxy)benzoyloxy)biphenyl-4-yl 6-(perfluorooctanoyloxy)hexahydrofuro[*3,2-b*]furan-3-yl adipate (**UBPHA**) is identical to the one of **ABPHA**.

6-Oxo-6-(4′-(4-(undec-10-enoyloxy)benzoyloxy)biphenyl-4-yloxy)hexanoic acid is prepared by use of 4′-hydroxybiphenyl-4-yl 4-(undec-10-enoyloxy)benzoate and adipoyl dichloride. Yield: 81%. m.p.: 162 °C. IR (KBr, cm^{-1}): 3075, 2925, 2852 (CH_3, $-CH_2-$ and −CH−), 2640−2530 (−OH in −COOH), 1755, 1717, 1686 (C=O), 1641 (C=C on terminal olefinic group), 1608, 1493 (Ar), 1278 (C−O). Anal. Calcd for $C_{36}H_{40}O_8$: C, 71.98%; H, 6.71%. Found: C, 71.92%; H, 6.69%. ^{1}H NMR ($CDCl_3$, δ, ppm): 1.11−1.69 [m, 16H, $CH_2{=}CHCH_2(C\underline{H}_2)_6CH_2COO-$ and $-OOCCH_2(C\underline{H}_2)_2CH_2COO-$]; 2.01−2.16 [m, 2H, $CH_2{=}$

$\mathrm{CHC\underline{H}_2(CH_2)_6CH_2COO-}$]; 2.30–2.56 [m, 6H, $\mathrm{CH_2{=}CHCH_2(CH_2)_6C\underline{H}_2COO-}$ and $\mathrm{-OOCC\underline{H}_2(CH_2)_2C\underline{H}_2COO-}$]; 4.91–5.14 (m, 2H, $\mathrm{C\underline{H}_2{=}CH-}$); 5.93–6.11 (m, 1H, $\mathrm{CH_2{=}C\underline{H}-}$); 7.07–8.14 (m, 12H, Ar–$\underline{\mathrm{H}}$); 12.11–12.22 (S, 1H, -COO$\underline{\mathrm{H}}$).

6-Hydroxyhexahydrofuro[*3,2-b*]furan-3-yl 4′-(4-(undec-10-enoyloxy)benzoyloxy)biphenyl-4-yl adipate is synthesized using 4′-(6-chloro-6-oxohexanoyloxy)biphenyl-4-yl 4-(undec-10-enoyloxy) benzoate and isosorbide. Yield: 61%. m.p.: 82 °C. IR (KBr, cm^{-1}): 3441 (–OH), 3075, 2925, 2852 ($\mathrm{CH_3}$, $\mathrm{-CH_2-}$, –CH– and Ar–H), 1758-1721 (C=O), 1602, 1494 (Ar) 1274, 1206, 1164 (C–O). Anal. Calcd for $\mathrm{C_{42}H_{48}O_{11}}$: C, 69.21%; H, 6.64%. Found: C, 69.73%; H, 6.62%. ^{1}H NMR ($\mathrm{CDCl_3}$, δ, ppm): 1.14–1.73 [m, 16H, $\mathrm{CH_2{=}CHCH_2(C\underline{H}_2)_6CH_2COO-}$ and $\mathrm{-OOCCH_2(C\underline{H}_2)_2CH_2COO-}$]; 2.10–2.19 [m, 2H, $\mathrm{CH_2{=}CHC\underline{H}_2(CH_2)_6CH_2COO-}$]; 2.29–2.58 [m, 6H, $\mathrm{CH_2{=}CHCH_2(CH_2)_6C\underline{H}_2COO-}$ and $\mathrm{-OOCC\underline{H}_2(CH_2)_2C\underline{H}_2COO-}$]; 3.64–4.69 [m, 8H, $\mathrm{-C\underline{H}_2-O-}$ and $\mathrm{-C\underline{H}-O-}$ in isosorbide group]; 4.90–5.12 (m, 2H, $\mathrm{C\underline{H}_2{=}CH-}$); 6.03–6.18 (m, 1H, $\mathrm{CH_2{=}C\underline{H}-}$); 7.15–8.11 (m, 12H, Ar–$\underline{\mathrm{H}}$); 9.37–9.49 (S, 1H, –O$\underline{\mathrm{H}}$).

Liquid crystalline monomer **UBPHA** is prepared from 6-hydroxyhexahydrofuro[*3,2-b*]furan-3-yl 4′-(4-(undec-10-enoyloxy) benzoyloxy)biphenyl-4-yl adipate and perfluorooctanoyl chloride. Yield: 51%. $[\alpha]_D^{20} = +40.2°, c = 1$, chloroform; m.p.: 61.0 °C. IR (KBr, cm^{-1}): 3075, 2928, 2854 ($\mathrm{-CH_3}$-, $\mathrm{-CH_2}$-, –CH– and Ar–H), 1760–1724 (C=O), 1603, 1495 (Ar), 1272, 1258, 1207, 1166 (C–O–C), 1146 (C–F). Anal. Calcd for $\mathrm{C_{50}H_{47}F_{15}O_{12}}$: C, 53.39%; H, 4.21%. Found: C, 53.33%; H, 4.17%. ^{1}H NMR ($\mathrm{CDCl_3}$, δ, ppm): 1.21–1.75 [m, 16H, $\mathrm{CH_2{=}CHCH_2(C\underline{H}_2)_6CH_2COO-}$ and $\mathrm{-OOCCH_2(C\underline{H}_2)_2CH_2COO-}$]; 2.05–2.18 [m, 2H, $\mathrm{CH_2{=}CHC\underline{H}_2(CH_2)_6CH_2COO-}$]; 2.48–2.62 [m, 6H, $\mathrm{CH_2{=}CHCH_2(CH_2)_6C\underline{H}_2COO-}$ and $\mathrm{-OOCC\underline{H}_2(CH_2)_2C\underline{H}_2COO-}$]; 3.69–4.21 [m, 8H, $\mathrm{-C\underline{H}_2-O-}$ and $\mathrm{-C\underline{H}-O-}$ in isosorbide group]; 4.91–5.13 (m, 2H, $\mathrm{C\underline{H}_2{=}CH-}$); 5.79–5.93 (m, 1H, $\mathrm{CH_2{=}C\underline{H}-}$); 6.98–8.16 (m, 12H, Ar–$\underline{\mathrm{H}}$).

2.3. Synthesis of the liquid crystalline resins

The side-chain liquid crystalline resins are prepared from LC monomers **ABPHA** and **UBPHA**, epoxy compound **AMO** and commercially available **PMHS** with an averaged degree of polymerization of 35. Fig. 2 shows the synthesis of the resins and elastomers, and the polymerization experiments are summarized in Table 1. The synthesis of polymer **PI-2** is given as an example. Liquid-crystalline monomer **ABPHA** (2.31 g, 2.31 mmol) and the epoxy compound **AMO** (0.14 g, 1.19 mmol) is dissolved in 30 mL of dry, fresh distilled toluene. To the stirred solution, **PMHS** (0.23 g, 0.10 mmol) and 2 mL of a 0.5% hexachloroplatinic (THF solution) are added and heated under nitrogen and anhydrous conditions at 65–68 °C for 30 h. Then 20 mL of the solvent is distilled out, and the residue is cooled to room temperature and poured into 100 mL methanol. The product is filtered off, dissolved in chloroform and precipitated in methanol (3 times), and dried at 80 °C under vacuum for 24 h to obtain 2.49 g of liquid crystalline resin **PI-2**. Yield: 93%. The specific rotation ($[\alpha]_D^{20}$) and the epoxy value are listed in Table 1. IR (KBr, cm^{-1}): 2928, 2852 (C–H aliphatic), 1785–1716 (C=O in different ester linkages), 1607, 1510 (Ar), 1273, 1169 (C–O–C), 1146 (C–F), 1023 (Si–O). ^{1}H NMR ($\mathrm{CDCl_3}$, δ, ppm): 0–0.20 (s, 1.14H, Si–CH_3); 0.41–0.53 (m, 0.69H, Si–CH_2–); 1.22–2.58 (m, 3.28H, alkyl-H); 3.78–4.47 [m, 3.13H, $\mathrm{-C\underline{H}_2-O-}$ and$\mathrm{-C\underline{H}-O-}$]; 7.08–8.16 (m, 2.76H, Ar–$\underline{\mathrm{H}}$).

2.4. Preparation of the orientated liquid crystalline elastomers

Liquid crystalline resins are cured by mechanically mixing the epoxy resins and curing agent **DDM** without any solvent, taken in a stoichiometric ratio (2:1) according to the epoxy value of the resins in Table 1. Each mixture is heated to 98 °C and stirred for 10 min at this temperature, to make it homogeneous. The epoxy resins and the curing agent are miscible when they were mechanical mixed, and the mixture turn white during the mixing. Successively, it is poured between two glass slides and cured under magnetic fields of 10 T at 98 °C, and the crosslinking reaction is monitored by measuring the FTIR spectra. The FTIR spectroscopy is used to detect the curing process previously [31].

3. Results and discussion

3.1. Preparation and characterization

The chemical structures of **ABPHA**, **UBPHA** and the liquid crystalline resins are characterized by FTIR and ^{1}H NMR spectra. The liquid-crystalline monomers **ABPHA** and **UBPHA** are prepared by etherification of perfluorooctanoyl chloride and hydroxyl compound. In the ^{1}H NMR spectra attribute analysis of **ABPHA** and **UBPHA**, the chemical shift values nearby 1.2–2.9, 4.8–5.6, 5.8–6.2 and 7.0–8.2 ppm correspond to the characteristic protons in the monomers such as methylene protons, olefinic protons, and aromatic protons, respectively. IR spectra of **ABPHA** and **UBPHA** display characteristic weak peaks near 3060 and 1640 cm^{-1} attributable to C–H and C=C stretching on terminal olefinic groups, and strong peaks near 1760–1724, 1608–1495, 1145–1149 cm^{-1} corresponding to C=O, aromatic C=C and C–F stretching bands respectively. The structure characterization and elemental analysis of the monomers are in good agreement with the prediction.

Table 1
Polymerization, specific rotation analyses, WAXD data, and order parameter of the samples.

sample	monomer composition in feed[a]			α[b]	Epoxy value[c]	WAXD Data	order parameter ***S***
	ABPHA (mmol)	**UBPHA** (mmol)	**AMO** (mmol)	(°)	(mmol/g)	2θ (deg) [intensity (a.u.)]/D-spacing (Å)[d]	
PI−1	2.91	0	0.59	+ 38.8	0.197	2.70^s[6200]/32.7, 4.98^s[1800]/17.7, 16.42^b[4100]/5.4	
PI−2	2.31	0	1.19	+ 35.2	0.485	2.74^s[5900]/32.2, 5.12^s[1800]/17.3, 16.84^b[3600]/5.3	
PII−1	0	2.91	0.59	+ 37.6	0.175	2.49^s[6500]/35.5, 4.73^s[1250]/18.7, 16.49^b[1950]/5.4	
PII-2	0	2.31	1.19	+ 34.7	0.434	2.84^s[9100]/31.1, 5.22^s[2200]/16.9, 16.94^b[4200]/5.2	
EI−1						2.61^s[13,100]/33.8, 4.98^s[1800]/17.7, 16.70^b[3000]/5.3	0.84
EI−2						2.74^s[27,500]/32.2, 5.07^s[2200]/17.4, 16.41^b[4100]/5.4	0.76
EII−1						2.63^s[21,000]/33.6, 5.21^s[1600]/17.0, 17.72^b[4100]/5.0	0.87
EII-2						2.70^s[31,000]/32.7, 5.11^s[2900]/17.3, 16.89^b[3100]/5.2	0.78

[a] based on 0.1 mmol of the starting poly(methylhydrogeno)siloxane (**PMHS**) for each sample.
[b] specific rotation of resins, 0.1 g in 10 mL $\mathrm{CHCl_3}$.
[c] the epoxy value is measured via hydrogen bromide-acetic acid titrimetric analysis.
[d] WAXD peak shape: s, sharp; b, broad; intensity, the maximum peak height. All the samples are measured at 80 °C.

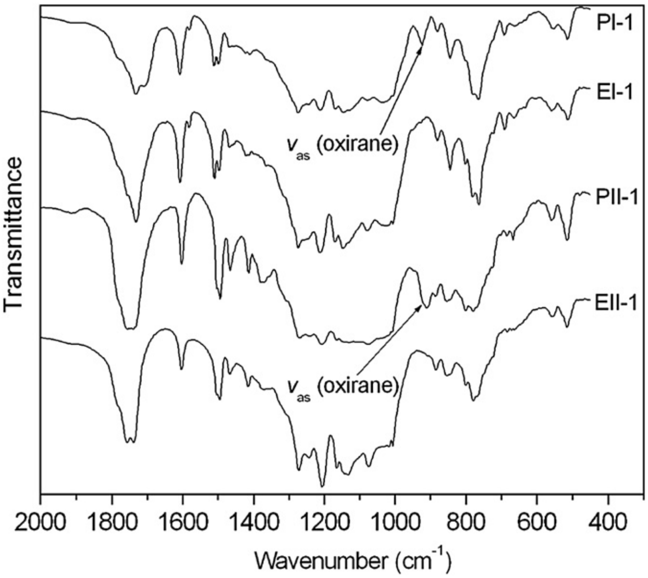

Fig. 3. FTIR spectra of representative polymers PI-1, PII-1, EI-1 and EII-1.

The side-chain liquid crystalline resins **PI-1**, **PI-2**, **PII-1** and **PII-2** are prepared by a one-step hydrosilylation reaction between Si–H groups of **PMHS** and terminal olefinic $CH_2{=}CH-$ of LC monomers **ABPHA** and **UBPHA**, epoxy compound **AMO** in anhydrous toluene, using hexachloroplatinic acid as catalyst. The specific rotations of the liquid crystalline resins **PI-1**, **PI-2**, **PII-1** and **PII-2** are given in Table 1, indicating that the polysiloxanes show lower specific rotation absolute values in comparison with monomers. It suggests that cleavage of the terminal olefinic bond and the binding of monomers to the polysiloxane main chains affect the chirality of the polysiloxanes.

The orientated liquid crystalline elastomers **EI-1**, **EI-2**, **EII-1** and **EII-2** are prepared by curing of the corresponding liquid crystalline resins **PI-1**, **PI-2**, **PII-1** and **PII-2** with a curing agent under magnetic fields. The crosslinking reaction is monitored by measuring the FTIR spectra of the film, as shown in Fig. 3. A reduction of the epoxide group concentration is verified for all samples by observing the infrared absorption peak at 920 cm^{-1}, which is due to the asymmetric stretch of the oxirane ring. Absence of characteristic epoxy peak peaks for **EI-1**, **EI-2**, **EII-1** and **EII-2** suggests that the crosslinking reaction is thoroughly finished.

3.2. Liquid crystalline monomers

The olefin compound **ABPHA** and **UBPHA** containing chiral and terminal perfluorocarbon-chain units display enantiotropic mesophases including S_c^* and N^* phases. The transition temperatures and corresponding enthalpy changes (ΔH) are displayed in Fig. 4.

The DSC curves of LC monomer **ABPHA** show a crystalline melting endotherm at 64.4 °C ($\Delta H = 14.48$ J g^{-1}), a S_c^*–N^* transition at 126.4 °C (0.09 J g^{-1}) and mesogenic-isotropic phase transition at 209.4 °C (16.59 J g^{-1}) on heating, as well as a isotropic–mesogenic transition at 198.5 °C (−8.49 J g^{-1}), a N^*–S_c^* transition at 139.5 °C (−0.73 J g^{-1}) and crystallization at 55.5 °C (−2.37 J g^{-1}) on cooling. Comparing with the enthalpy changes of melting and S_c^*–N^* transition, enthalpy change of the mesogenic-isotropic phase transition is the greatest, suggesting influence of terminal perfluorocarbon chains unit. The strong self-segregation of fluorinated segments and the rigid-rod-like nature of fluorocarbon chains tend to adopt a stabilized conformation in the mesophase state. Thus the phase transition from mesophase to isotropic phase in the hydrocarbon-perfluorocarbon systems needs more energy. Observed by POM, **ABPHA** exhibited S_c^* and N^* textures upon heating and cooling circles, as illustrated in Fig. 5. Oily streak texture is one of the most commonly observed textures of the chiral nematic phase prepared between two untreated glass substrates. These oily streaks can be seen as a network of defect lines dispersed in uniformly helical regions. Influenced by self-segregation of fluorinated segments, these actual oily streaks appeared in large bundles as shown in Fig. 5a. When the isotropic state is cooled, cholesteric droplets of N^* phase separated from the isotropic melt, and different colors correspond to different twist states as displayed in Fig. 5b. On further cooling, a fan-shaped texture of S_c^* phase with an equidistant line pattern is displayed in Fig. 5c, which is due to the helical superstructure.

Compared with **ABPHA**, the monomer **UBPHA** possesses longer hydrocarbon chain on the other terminal side of the molecules. The DSC curves and the enthalpy changes of **UBPHA** are similar to those of **ABPHA**, as illustrated in Fig. 4. These results suggest that the length of the terminal hydrocarbon chain can't influence greatly to the liquid crystalline systems with another terminal perfluorocarbon chains. However, **UBPHA** shows a little different from **ABPHA** when it is observed by POM. Fig. 5d displays cholesteric droplets from the isotropic melt. As the droplets grow larger, they are superimposed by the equidistant line pattern due to the S_c^* helix, showing a focal conic texture as seen in Fig. 5e. This suggests

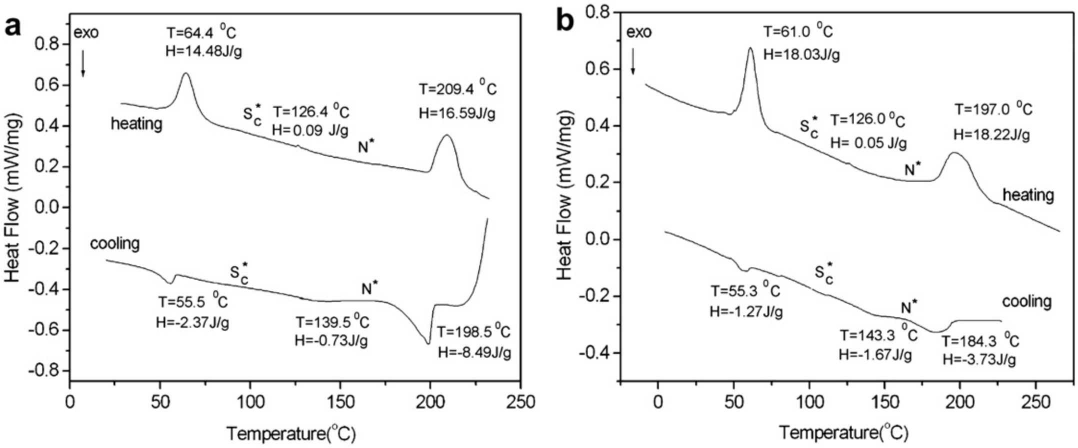

Fig. 4. DSC thermograms for (a) 4′-(4-(allyloxy)benzoyloxy)biphenyl-4-yl 6-(perfluorooctanoyloxy)hexahydrofuro[3,2-*b*]furan-3-yl adipate (ABPHA); and (b) 4′-(4-(undec-10-enoyloxy)benzoyloxy)biphenyl-4-yl 6-(perfluorooctanoyloxy)hexahydrofuro[3,2-*b*]furan-3-yl adipate (UBPHA).

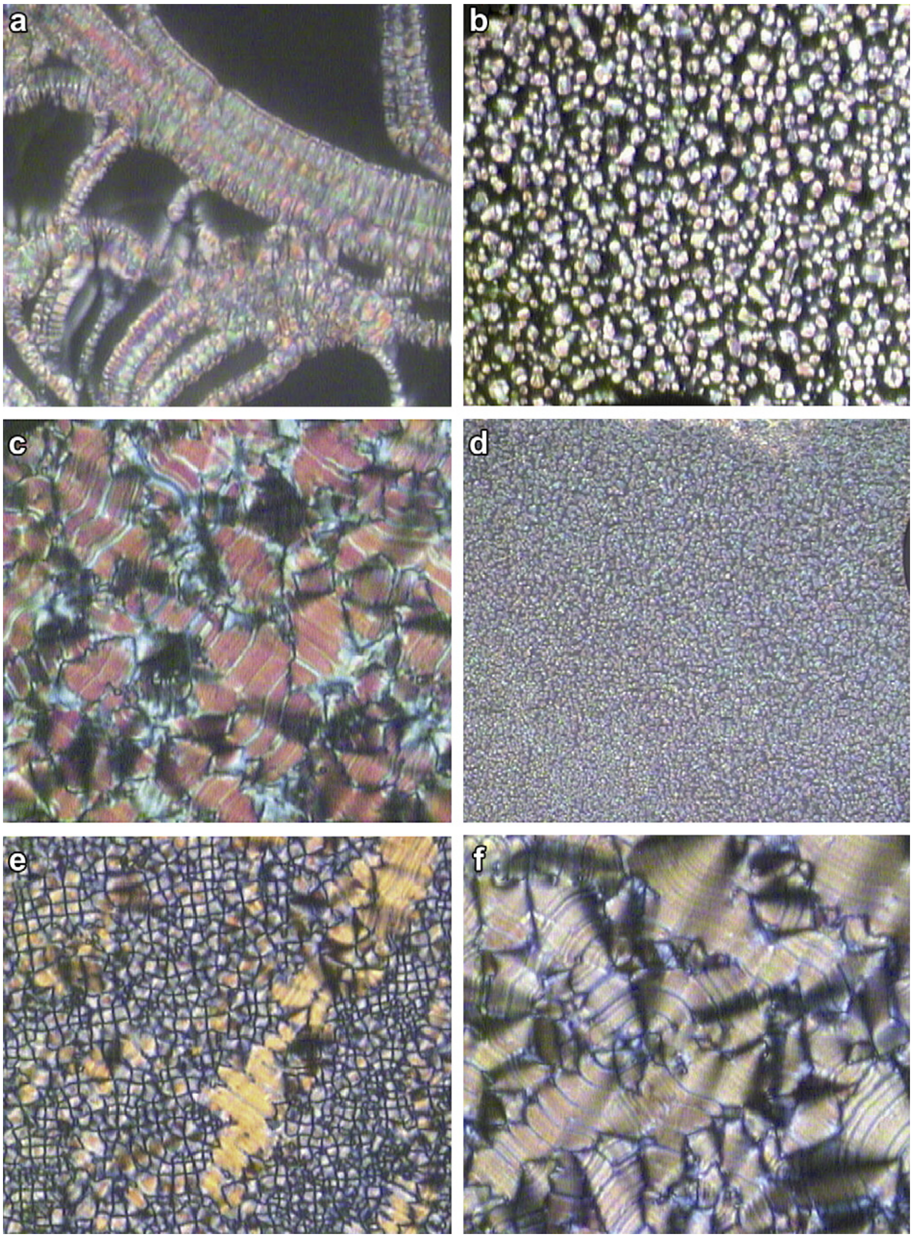

Fig. 5. Optical texture of the monomers (200 ×): (a) oily-streak texture (N^*) of 4′-(4-(allyloxy)benzoyloxy)biphenyl-4-yl 6-(perfluorooctanoyloxy)hexahydrofuro[*3,2-b*]furan-3-yl adipate (ABPHA) on heating to 194 °C; (b) cholesteric droplets of ABPHA on cooling to 193 °C; (c) striped fan-shape texture (S_c^*) for ABPHA on cooling to 118 °C; (d) cholesteric droplets of 4′-(4-(undec-10-enoyloxy)benzoyloxy)biphenyl-4-yl 6-(perfluorooctanoyloxy)hexahydrofuro[*3,2-b*]furan-3-yl adipate (UBPHA) on cooling to 181 °C; (e) focal conic texture of UBPHA on cooling to 141 °C; (f) striped fan-shape texture (S_c^*) for UBPHA on cooling to 128 °C.

that the helix axes of the cholesteric and the S_c^* phases are perpendicular to each other. On further cooling, a striped fan-shape texture of S_c^* phase is also displayed for **UBPHA** in Fig. 5f.

3.3. Liquid crystalline resins

Thermal analysis of resins has been employed by TGA and DSC. It suggests high thermal stability in consideration of greater than 300 °C of onset weight loss temperatures (T_d) for **PI-1**, **PI-2**, **PII-1** and **PII-2**. DSC thermograms of the resins on heating cycles are displayed in Fig. 6a. All the epoxy resins **PI** and **PII** series display glass transition, S_c^*–N^* mesophase transition and N^*-isotropic phase transition on heating. With regard to the variation of mesophasic transition temperatures of epoxy resins **PI-1**, **PI-2**, **PII-1** and **PII-2**, the isotropization temperatures and mesophasic ranges are reduced as the perfluorocarbon chains decreased. The glass transition temperature (T_g) of all epoxy resins are showed near 50 °C, but the mesophase-isotropic phase transition temperature (T_i) of the **PI** and **PII** series of resins decreased slightly with increase of epoxy compound **AMO** component in the polymer systems, suggesting reduced mesophasic ranges for **PI-2** and **PII-2** in comparison with **PI-1** and **PII-1**. The enthalpy changes of S_c^*–N^* transition for **PI-1**, **PI-2**, **PII-1** and **PII-2** are higher than those of corresponding monomers **ABPHA** and **UBPHA**. This can be explained by the bound state of mesogens in the polymer systems. In contrast to the monomers, the mesogenic units bearing terminal fluorocarbon chains are surrounded by the polymer matrix in S_c^* mesophase, resulting in increase of enthalpy changes.

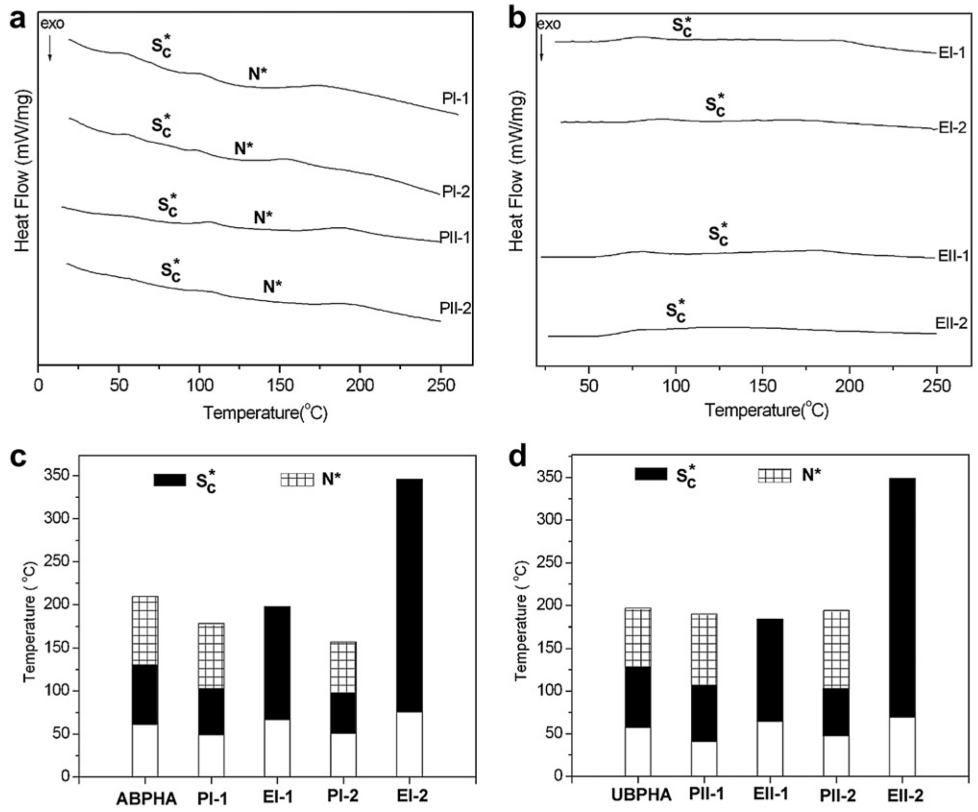

Fig. 6. DSC thermograms of (a) resins upon second heating and (b) elastomers upon first heating, and phase diagrams of (c) EI elastomers (including originated monomer ABPHA and the resins) and (d) EII elastomers (including originated monomer UBPHA and the resins).

The optical textures of the epoxy resins are studied by use of POM with hot stage, and some representative optical textures are shown in Fig. 7. Fig. 7a shows a oily-streak texture of chiral nematic (N^*) phase of **PI-1** at 165 °C in heating process, and the oily-streak texture is due to horizontal (homeotropic) alignment of mesogenic core in N^* phase. Fig. 7b displays a line texture of chiral smectic C (S_c^*) phase of **PI-2** at 95 °C in heating process. The helix lines are parallel to the smectic layer planes and the helix axis is perpendicular to the lines, i.e. the smectic layer plane. For **PII-1**, it shows a striped fan-shape texture (S_c^*) on heating to 105 °C Fig. 7c, which is superimposed by an equidistant line pattern due to the helical superstructure when passing into S_c^* phase. Fig. 7d displays a parabolic texture (S_c^*) of **PII-2** on cooling to 92 °C, and a little lines appeared in the textures suggest the helix structure of the polymer.

In these epoxy resins, the S_c^* phase can be detected from DSC and optical microscopic methods, but it is more definitely detected from an estimation of layer spacing by X-ray measurements. X-ray studies are carried out to obtain some detailed information on LC phase structure, and some WAXD data of all the samples are summarized in Table 1. A broad reflection at wide angles (associated with the lateral packings) and sharp reflection at small angles (associated with the smectic layers) are separately shown by all the profile curves of resins **PI-1**, **PI-2**, **PII-1** and **PII-2** when the samples are heated above glass transition temperature. Fig. 8a shows a one-dimensional WAXD powder pattern of **PII-1**, providing structural information on two length scales. One is on the nanometer scale in the low 2θ angle region at 2.49° (d-spacing = 3.55 nm), and the other is on the subnanometer scale at 16.49° (d-spacing = 0.54 nm). They can be assigned as the average lateral distance (5.4 Å) between molecules and the average length (35.5 Å) of the repeat units with short-range order. From molecular models the side-chain length of these polysiloxanes to give smectic layers can be calculated, and for **PII-1** it is approximately 46.4 Å. The X-ray diffraction data show the layer periodicity is nearly 35.5 Å and the ratio of the observed layer spacing (***d***) to the calculated lengths (***L***) is 0.765, showing that the side chains are located on one side of the main chain. Because the measured ***d*** is relatively smaller than the calculated ***L***, the LC side chains should be tilted to the layer to form a S_c^* phase. The tilt angle is estimated nearly 40°, which can be calculated from a relative ratio of ***d*** and ***L***. This result indicates synergistic effect between chiarl isosorbide groups and helical conformation of the rigid-rod-like nature of fluorocarbon chains. On further heating, the sharp reflection of d-spacing 35.5 Å became diffuse and weakly, verifying the S_c^*–N^* transition of the samples.

3.4. Oriented liquid crystalline elastomers

TGA thermograms of the oriented elastomers show high thermal stability in consideration of greater than 300 °C of onset weight loss temperatures (T_d) for **EI-1**, **EI-2**, **EII-1** and **EII-2**. Fig. 6b shows DSC thermograms of the oriented elastomers on heating cycles. All the elastomers **EI-1**, **EI-2**, **EII-1** and **EII-2** display glass transition and S_c^* phase, but isotropic transition is not shown distinctly for **EI-2** and **EII-2** on heating. In comparison with corresponding epoxy resins, S_c^*–N^* transition disappeared for the elastomers because of orientation and crosslinking process. The S_c^* mesophasic ranges for the oriented elastomers became greater than those for corresponding epoxy resins, as shown in Fig. 6c and d. The optical textures of the elastomers didn't change almost when the samples are heated from room temperature to decomposition temperature, as shown in Fig. 7e and f. For all the oriented elastomers, the formation of a periodic stripe pattern by application of

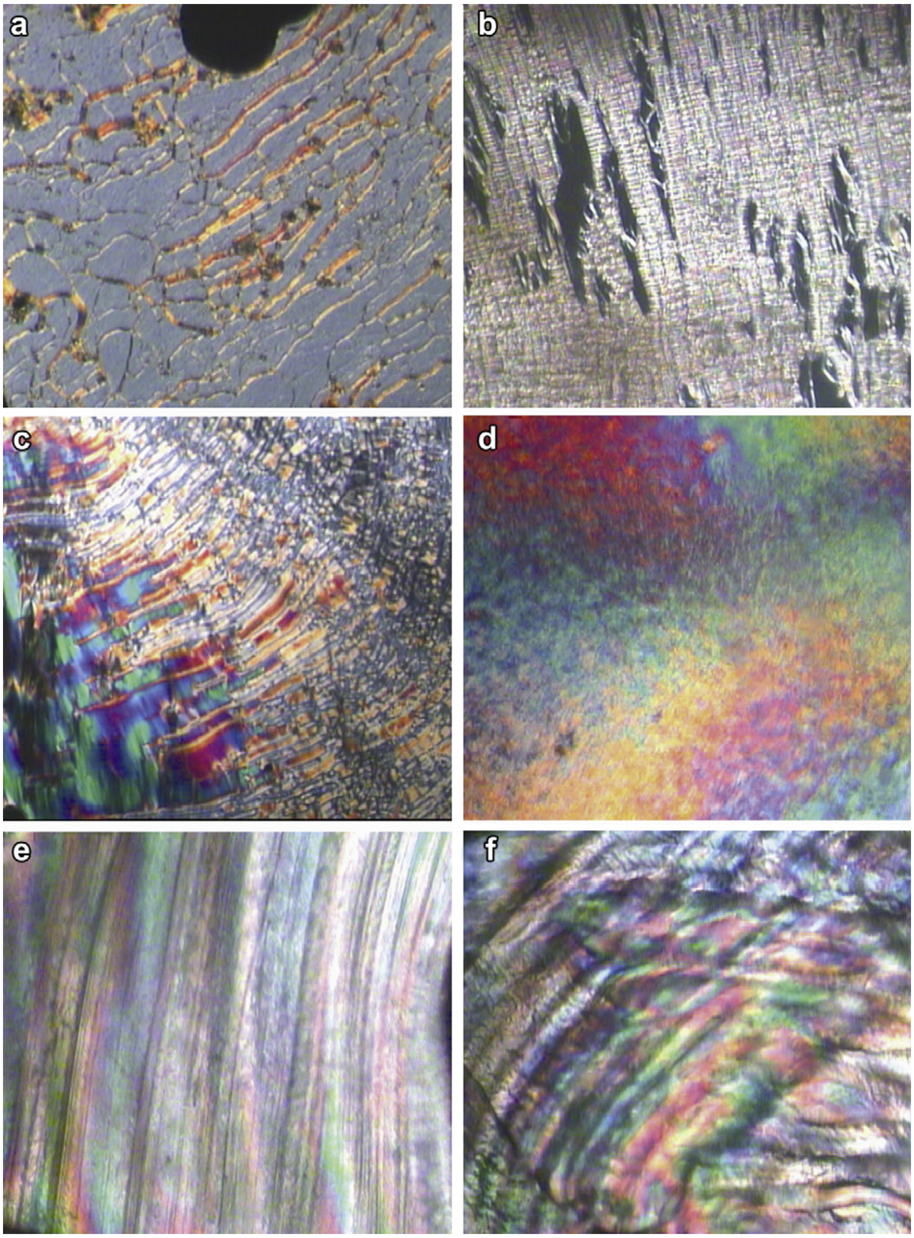

Fig. 7. Optical texture of the liquid crystalline resins (200 ×): (a) oily-streak texture (N^*) of PI-1 at 165 °C in heating process, (b) line texture of chiral smectic C (S_C^*) phase of PI-2 at 95 °C in heating process, (c) striped fan-shape texture (S_C^*) of PII-1 on heating to 105 °C, (d) parabolic texture (S_C^*) of PII-2 on cooling to 92 °C, (e) magnetic field induced striped domain texture (S_C^*) of EI-1, (f) magnetic field induced striped domain texture (S_C^*) of EII-2.

a magnetic field can be observed by POM, and the periodic stripe texture can be frozen via crosslinking reaction. These results indicate that the perfluorocarbon chains stabilize the S_C^* mesophase owing to the strong self-segregation of fluorinated segments and the rigid-rod-like nature of fluorocarbon chains in the crosslinking polymer systems. These can also be verified by X-ray method, and some WAXD data of all the oriented elastomers are listed in Table 1. Fig. 8b illustrates a WAXD curve of **EII-1**. A broad reflection at wide angles ($2\theta \approx 17^\circ$) and a strong sharp reflection at small angles ($2\theta \approx 2.7^\circ$) are shown in the profile curves of **EI-1**, **EI-2**, **EII-1** and **EII-2**, and are similar to those of corresponding epoxy resins **PI-1**, **PI-2**, **PII-1** and **PII-2**, as displayed in Table 1. But the maximum peak heights at small angles (near 2.7°) of the elastomers are much greater than those of corresponding epoxy resins (see Fig. 8c). Because the reflections near 2.7° corresponds to the interlayer distances, the larger intensity of these peaks suggests the stronger regularity between the layer spacing. Because the measured layer spacing $\boldsymbol{d}$ is relatively smaller than the calculated lengths $\boldsymbol{L}$, the LC side chains should be tilted to the layer to form a S_C^* phase for all the elastomers, indicating nearly 40° of a tilt angle calculated from a relative ratio of $\boldsymbol{d}$ and $\boldsymbol{L}$.

For the oriented elastomers **EI-1**, **EI-2**, **EII-1** and **EII-2**, the average degree of orientation of the LC domains can be represented by the orientation parameter, ***S***, which is defined according to eq:

$$\boldsymbol{S} = \left(3 < \cos^2\boldsymbol{\varphi} > -1\right)\Big/2 \qquad (1)$$

where ϕ is the angle between the individual domain directors and the orientation direction, and $< >$ denotes an average of $\cos^2\boldsymbol{\varphi}$ over all the LC domains. The order parameters of the LCEs are

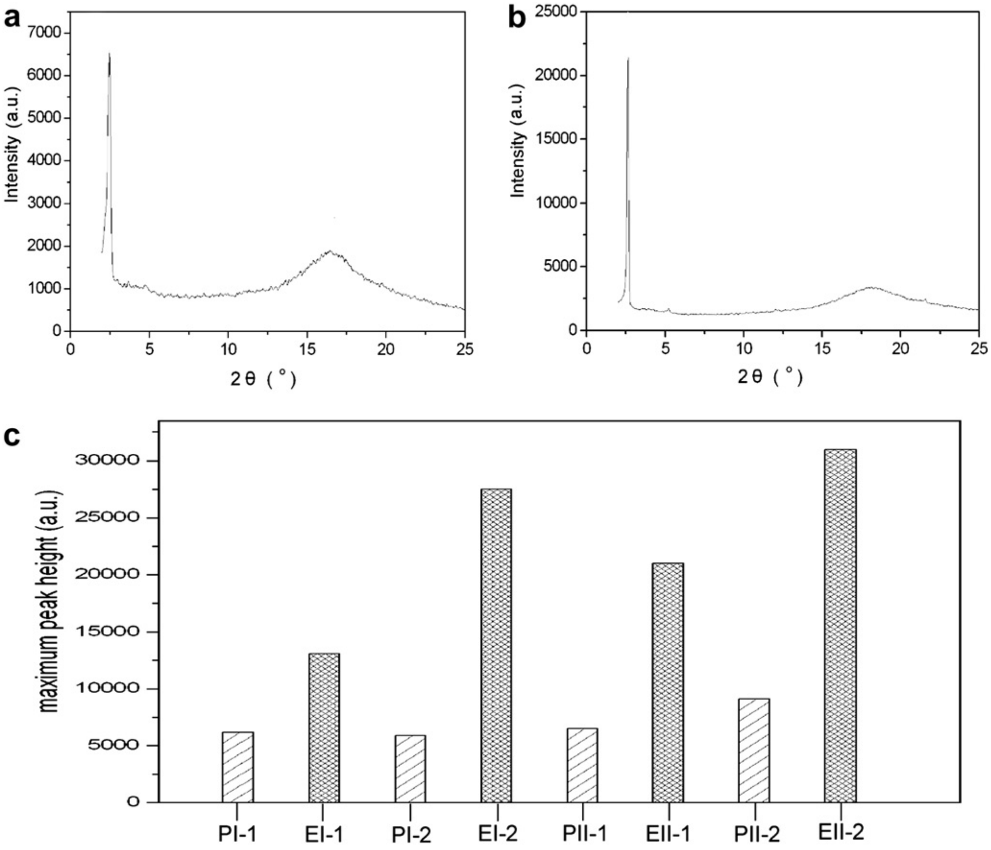

Fig. 8. WAXD curves of (a) epoxy resin PII-1 and (b) crosslinked oriented elastomers EII-1, and (c) the maximum peak heights of the resins and elastomers at small angles.

determined by X-ray measurements, which are listed in Table 1. Fig. 9a shows a two-dimensional SAXS pattern of the sample **EII-1** at room temperature. The macroscopic layer thickness can be determined by use of SAXS measurements. The two-dimensional SAXS patterns of the oriented LCEs display quadrants, providing structural information on two aspects. On the one hand, the scattering patterns confirm the smectic mesophase. As a rule, nematic liquid crystalline polymers show no scattering information in SAXS pattern, but smectic liquid crystalline polymers display scattering patterns. In addition, the greater scattering angles suggest that layer thickness is minor, indicating the tilted structure for the S_C^* phase. On the other hand, the quadrant patterns should be originated from orientation of the elastomers. For the LCEs, the rigid-rod-like fluorocarbon chains tend to form layers due to poor miscible between fluorocarbons and hydrocarbons. Thus both the terminal fluorocarbon chains and the mesogenic groups constitute rigid units in the LCEs. As a result, the tilted rigid units cause tilted scattering patterns. The schematic of the macroscopic orientation is shown in Fig. 9b.

The four-spot small-angle pattern in Fig. 9 suggests that the oriented elastomers have a conical distribution of smectic layer normals around the director similar to some reported chiral and achiral smectic C main-chain LCEs [32,33]. The conical distribution of the layer normals is reflected in the splitting into 4 peaks with layer normals for chiral smectic C LCEs [32]. In these chiral smectic C LCEs, the smectic layer normal is not oriented parallel to the director but tilted by a tilt angle. As the samples were orientated and crosslinked under a magnetic field, a uniaxial deformation couples to the director orientation, resulting in a uniform director alignment parallel to the deformation axis and a conical distribution of the smectic layer normals around the director.

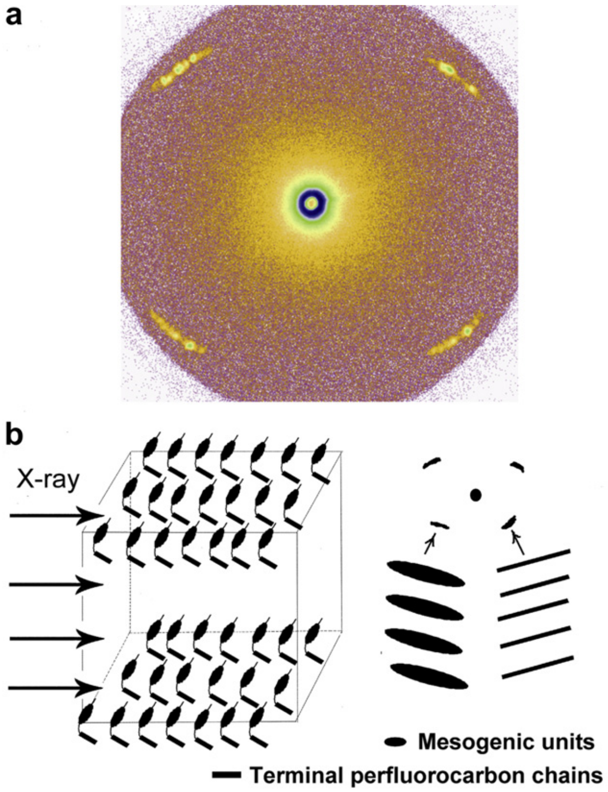

Fig. 9. Two-dimensional SAXS pattern of the sample EII-1 at room temperature (a) and the schematic of the macroscopic orientation (b).

4. Conclusions

Several novel side-chain liquid crystalline polysiloxane epoxy resins with various molar ratio of epoxy groups and mesogenic components are synthesized using liquid crystals bearing both chiral isosorbide units and terminal perfluorocarbon chains, and the epoxy resins are cured at mesophase state under a magnetic field to obtain crosslinked oriented elastomers. The mesomorphic properties in the side-chain comb-shaped liquid crystalline resins and their corresponding oriented elastomers are influenced by the terminal perfluorocarbon chains components effectively. Several kinds of chiral nematic and tilted smectic phases are obtained in the side-chain epoxy resins, and tilted smectic phases are frozen in their corresponding oriented elastomers. The LC phases are verified by X-ray measurements, and the orientational order parameters of the oriented LCEs are calculated.

Acknowledgments

The authors are supported by the Fundamental Research Funds for the Central Universities (N090405003 and N090105001), Program for New Century Excellent Talents in University and Project 50873018 supported by NSFC.

References

[1] Spillmann CM, Konnert JH, Deschamps JR, Naciri J, Ratna BR. Chem Mater 2008;20:6130–9.
[2] Qin H, Mather PT. Macromolecules 2009;42:273–80.
[3] Ambrogi V, Giamberini M, Cerruti P, Pucci P, Menna N, Mascolo R, Carfagna C. Polymer 2005;46:2105–21.
[4] Yang H, Buguin A, Taulemesse JM, Kaneko K, Mery S, Bergeret A, Keller P. J Am Chem Soc 2009;131:15000–4.
[5] Cordoyiannis G, Lebar A, Rozic B, Zalar B, Kutnjak Z. Macromolecules 2009;42:2069–73.
[6] Harada M, Okamoto N, Ochi M. J Polym Sci Part B Polym Phys 2010;48:2337–45.
[7] Beyer P, Terentjev EM, Zentel R. Macromol Rapid Comm 2007;28:1485–90.
[8] Kossack W, Papadopoulos P, Heinze P, Finkelmann H, Kremer F. Macromolecules 2010;43:7532–9.
[9] Gebhard E, Zentel R. Macromol Chem Phys 2000;201:902–10.
[10] Assender HE, Windle AH. Polymer 1996;37:371–5.
[11] Goto H, Akagi K, Itoh K. Synth Met 2001;117:91–3.
[12] Majewski PW, Osuji CO. Soft Matt 2009;5:3417–21.
[13] Nishikawa E, Yamamoto J, Yokoyama H, Finkelmann H. Macromol Rapid Commun 2004;25:611–7.
[14] Callau L, Reina JA, Mantecon A. J Polym Sci Part A Polym Chem 2003;41:3384–99.
[15] Meng FB, Chen HB, Liu D, Zhang BY, Jia C. Polym Advanc Tech 2009;20:972–80.
[16] Ren W, McMullan PJ, Griffin AC. Phys Status Solidi B 2009;246:2124–30.
[17] Zubarev ER, Kuptsov SA, Yuranova TI, Talroze RV, Finkelmann H. Liq Cryst 1999;26:1531–40.
[18] Luca GD, Rey AD. Eur Phys J E 2003;12:291–302.
[19] Ortiz C, Ober CK, Kramer EJ. Polymer 1998;39:3713–8.
[20] Patil HP, Lentz DM, Hedden RC. Macromolecules 2009;42:3525–31.
[21] Kremer F, Lehmann W, Skupin H, Hartmann L, Stein P, Finkelmann H. Polym Adv Technol 1998;9:672–6.
[22] Hiraoka K, Stein P, Finkelmann H. Macromol Chem Phys 2004;205:48–54.
[23] Tashiro T, Kondo Y, Hiraoka K. Macromol Rapid Commun 2010;31:1948–53.
[24] Hiraoka K, Kobayasi M, Kazama R, Finkelmann H. Macromolecules 2009;42:5600–4.
[25] Andruzzi L, Apollo FD, Galli G, Gallot B. Macromolecules 2001;34:7707–14.
[26] Kim BG, Chung JS, Sohn EH, Kwak SY, Lee JC. Macromolecules 2009;42:3333–9.
[27] Bertolucci M, Galli G, Chiellini E, Wynne KJ. Macromolecules 2004;37:3666–73.
[28] Bracon F, Guittard F, Givenchy ET, Cambon A. J Polym Sci Part A Polym Chem 1999;37:4487–94.
[29] Goto H, Dai X, Narihiro H, Akagi K. Macromolecules 2004;37:2353–9.
[30] Meng FB, Cui Y, Chen HB, Zhang BY, Jia C. Polymer 2009;50:1187–96.
[31] Ortiz C, Kim R, Rodighiero E, Ober CK, Kramer EJ. Macromolecules 1998;31:4074–88.
[32] Heinze P, Finkelmann H. Macromolecules 2010;43:6655–65.
[33] Sanchez-Ferrer A, Finkelmann H. Macromolecules 2008;41:970–80.